Chapter-2

Fabrication and Characterization of Thermally Grown $MoSe_2$ Thin-Film Based MSM Broadband Photodetector

The Part of the work is adopted from-

S. Singh and S. Jit, **"Thermally Grown $MoSe_2$ Thin Film Based MSM Broadband Photodetector.,"** ***IEEE Photonics Technology Letters*****,** vol. 36, no. 18, pp. 1105–1108, Sept. 15, 2024, doi: 10.1109/LPT.2024.3442969.

2.1 Introduction

As described in the previous chapter, broadband photodetectors exhibit a wide spectral detection range, covering UV-Visible or UV-Visible-IR regions [6], [82]. These devices continue to be in high demand due to their wide-ranging applications across various fields, including optical communication, thermal imaging, biomedical imaging, day/night surveillance, environmental monitoring, and more [6], [7], [36], [38]. Chapter 1 also discussed that transition metal dichalcogenides (TMDs) are promising photoactive materials for broadband photodetection due to their bandgap tunability with film thickness, high carrier mobility, excellent conductivity, and strong light-matter interaction characteristics [36], [43], [44], [56]. Among TMDs, $MoSe_2$ has been relatively less explored for broadband photodetector applications. Therefore, this chapter investigates the performance characteristics of a broadband photodetector based on an Ag/$MoSe_2$ thin film/Ag Metal-Semiconductor-Metal (MSM) structure. The MSM configuration is chosen due to its ease of fabrication, compatibility with other components, low dark current, short carrier transit time, and large photoactive area, all of which contribute to enhanced photoresponse characteristics [9], [13], [98]. A typical MSM device can be visualized as two back-to-back Schottky diodes on a semiconducting substrate [13].

$MoSe_2$ nanopowder was synthesized using a simple and cost-effective hydrothermal method, followed by thin-film deposition on a SiO_2-coated Si substrate using thermal evaporation. Interdigitated silver (Ag) electrodes were then deposited on the $MoSe_2$ film, also via thermal evaporation, to complete the MSM (Ag/$MoSe_2$ thin film/Ag) device structure. The

interdigitated electrode design provides a larger photo-absorption area and shorter carrier transit times due to the closely spaced fingers [13]. Our proposed device demonstrated broadband photoresponse across the 300–1100 nm spectral range. Key performance parameters, including responsivity, detectivity, external quantum efficiency (EQE), and transient response, were systematically evaluated. To the best of our knowledge, this is the first report on an MSM broadband photodetector based on $MoSe_2$ thin films. The structure of this chapter is as follows:

Section 2.2 describes the fabrication process of the proposed MSM photodetector, including $MoSe_2$ synthesis, thin-film deposition, and electrode fabrication. Section 2.3 explains the energy band diagram and the working principle of the device. Section 2.4 presents the material characterization results and performance evaluation of the broadband photodetector. Finally, Section 2.5 provides the concluding remarks of the chapter.

2.2 Experimental Details

2.2.1. Material Synthesis

All the precursors with high-purity (99.99%) used for the material synthesis and device fabrication were purchased from Sigma-Aldrich, USA. For the synthesis of our active material, $MoSe_2$ nano-powder, cost-effective and facile hydrothermal route was adopted. All the precursors including sodium molybdate dehydrate($Na_2MoO_4.2H_2O$), selenium powder and sodium borohydride ($NaBH_4$) were taken into their stoichiometric ratio and were dissolved in the 60 ml mixed solution of absolute ethanol and de-ionised water with volumetric ratio 1:1. This resultant solution was subjected to rigorous stirring of 15 min. and

then transferred into Teflon lined-stainless steel autoclave. The sealed autoclave was kept in an oven at a temperature of 200°C maintained for 48 hours. Thereafter, natural cooling was allowed at room temperature to extract the black coloured sediment from the bottom of Teflon-lined autoclave. Then the extracted sediment was washed thoroughly for 3-5 times in absolute ethanol and DI water subsequently through centrifugation. Finally, after annealing it at 60°C for 12 hours, [84] the obtained $MoSe_2$ nano-powder was ready for thin film deposition in the thermal evaporation unit.

2.2.2. Substrate Cleaning and SiO_2 Growth

The boron-doped p^+ Si substrates (resistivity, 2-7 Ω-cm) were cleaned using standard Radio Corporation of America (RCA)-1 followed by RCA-2 methods. Firstly, the Si substraes were dipped into soap solution, DI water, acetone and Isopropanol subsequently and were subjected to ultra-sonication for 10 min. each. Further, after thorough rinsing in running DI water (from Millipore, Milli-Q, USA), samples were dipped into the Pirhana solution (mixture of H_2SO_4 and H_2O_2 in the volumetric ratio of 40:60) for 10 min. in order to remove any residual impurities. Thereafter, the samples were rinsed thoroughly in DI water followed by HF solution treatment with 10:1 ratio of DI:HF for 10 min. to remove the native oxides, if any, from the surface of the Si substrates. Finally, the samples were rinsed thoroughly with DI water and dried in an oven for 10 min. in N_2 ambient. Before proceeding for the growth of SiO_2 on the cleaned Si substrates, they were placed in oxygen plasma cleaner for 10 min. Thereafter, the samples were then placed in the quartz chamber of the oxidation furnace subjected at temperature 1100 °C for ~4 hours for SiO_2 layer growth (~300 nm thickness) on

the Si substrates for device fabrication [9].

2.2.3. Device Fabrication

Firstly, the SiO_2 grown Si substrate were diced into 15x15 mm^2 square pieces followed by subsequent cleaning in soap solution, DI water, acetone, and isopropanol in ultrasonicator bath for 10 min. each. Thereafter N_2 drying, these samples were processed for plasma cleaning (Femto Science Inc., CUTE, South Korea) for 10 min in $Ar:O_2$ (50:50) ambient before loading the samples in the thermal evaporation unit (FL400 SMART COAT 3.0 A, Hind High Vacuum, India). Under the high vacuum of ~ 2.4×10^{-6} mbar inside the chamber, the as-synthesized $MoSe_2$ powder kept in boat was thermally evaporated to get deposited at the rate of 1.0 Å/sec on the SiO_2/Si substrate samples mounted on the substrate holder within the chamber [4], [8]. The resultant $MoSe_2$ thin film thickness over SiO_2/Si substrate was ~ 30 nm measured through F-20 Filmetrics, USA. The interdigitated Ag electrodes were deposited at a rate of 0.2 Å /sec over $MoSe_2$ thin film with effective area of ~0.1264 cm^2 and thickness of 100 nm[38]. The schematic flow diagram for Device fabrication is shown in **Figure 2.1.** The schematic structure of the proposed device and its photograph from top view are shown in **Figure 2.2** (a) and (b), respectively. **Figure 2.2** (c) shows the FE-SEM image of the $MoSe_2$ film at 400 nm resolution which illustrates the growth of a uniform $MoSe_2$ film over the SiO_2 layer.

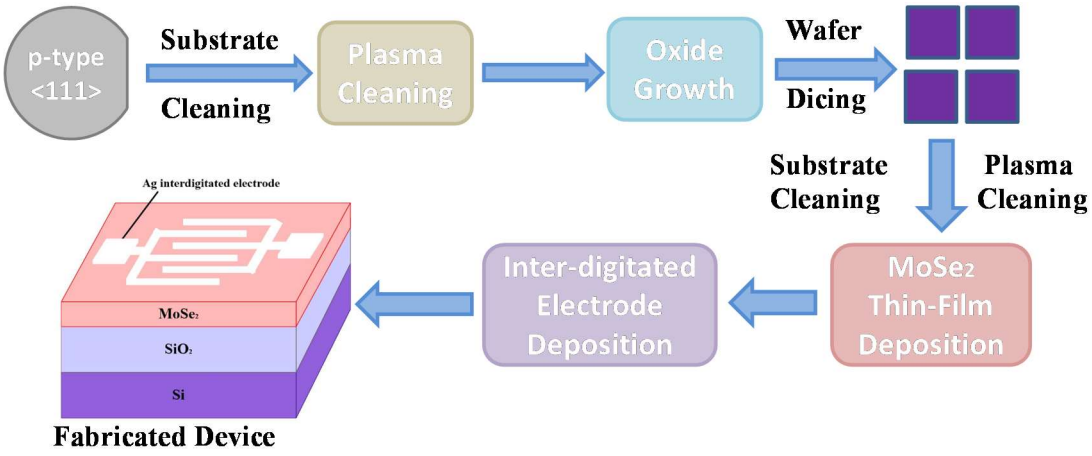

Figure 2.1 Schematic flow diagram for Device Fabrication.

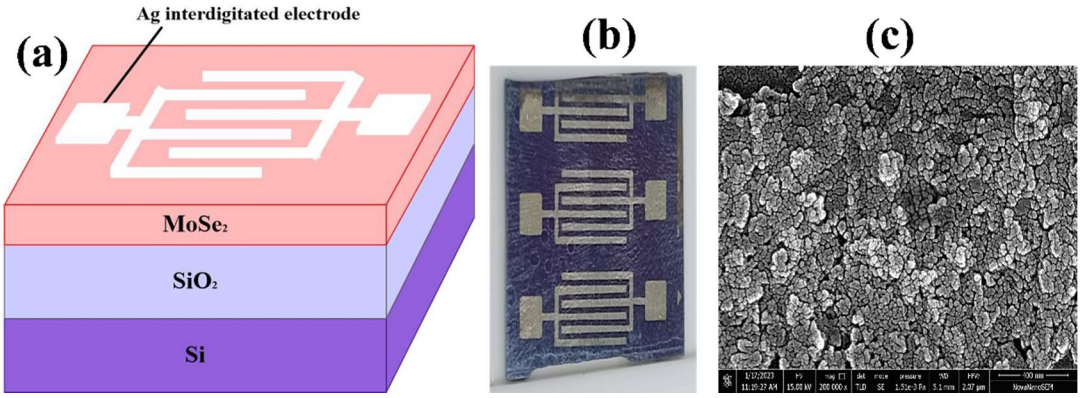

Figure 2.2 (a) Schematic device structure; (b) fabricated device image;(c) FE-SEM image of the $MoSe_2$ film.

2.3 Energy band diagram and Working of the device

The energy band diagram of our proposed device structure is illustrated in **Figure 2.3**. The energy band diagram before making the contacts shown in **Figure 2.3** (a) where the conduction band energy, valence band energy and work function of $MoSe_2$ are shown as −3.85 eV, −5.81 eV and −4.3 eV, respectively [99], and the work function of Ag metal electrodes as −4.6 eV (ϕ_M) [4]. Since $MoSe_2$ is intrinsically an n-type semiconductor, $\phi_M >$

ϕ_S confirms the Ag/$MoSe_2$ Schottky contact formation in the proposed MSM structure. **Figure 2.3** (b) shows the Fermi level alignment under equilibrium resulting into band bending due to formation of depletion regions inside $MoSe_2$ at two Ag/$MoSe_2$ Schottky junctions of the MSM device. When a bias voltage is applied one Schottky junction with +Ve side becomes forward biased while the other photodetector very small equal to the reverse saturation current of the Ag/MoSe2 Schottky junction. The resultant band diagram is shown in **Figure 2.3** (c). When light is incident on the device under an applied bias, photo-generated electron-hole pairs are directed in opposite directions as shown in **Figure 2.3** (c) which results in a photocurrent of the device [9], [98].

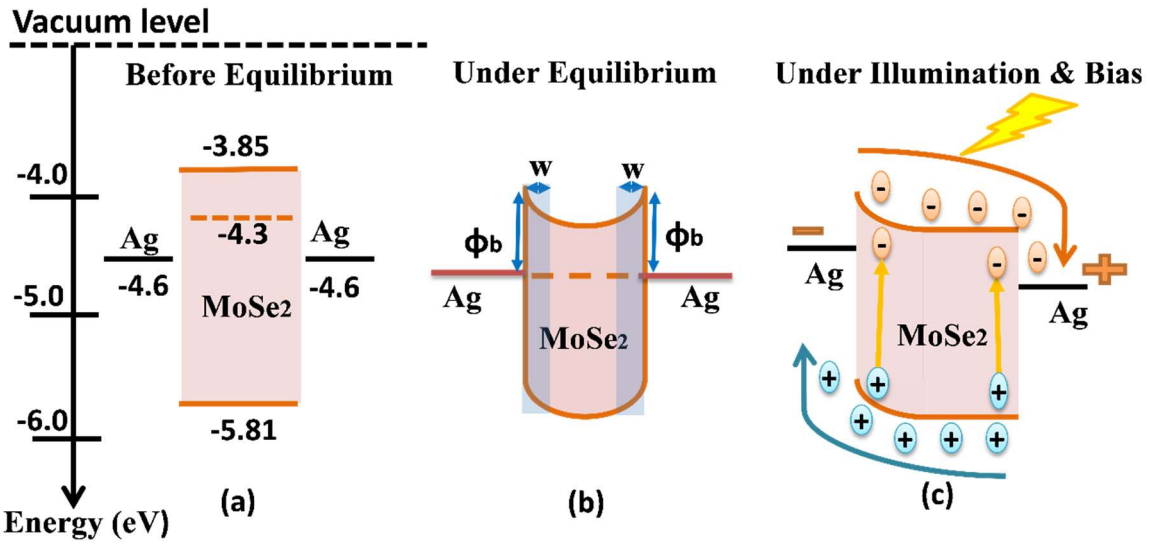

Figure 2.3 Energy band diagram of the proposed device (a) Before equilibrium; (b) Under equilibrium; (c) Under Illumination and Bias.

2.4 Results and Discussions

2.4.1. Material Characterization

The as-synthesized $MoSe_2$ powder was characterized for its cystallinity and phase purity through the X-ray Diffraction (XRD) system (Rigaku, SmartLab, 9kW, Cu-Kα radiation source (λ~1.5405 Å)) with 2θ scan range from 10° to 80°. **Figure 2.4** (a) shows the XRD pattern of the as synthesized material which is in good agreement with the previously reported works [48], [100]. It shows diffraction peaks(corresponding planes) at 13.6°(002), 27.3°(004), 31.94°(100), 38.26° (103), 46.8° (105), 56.2° (110), 65.81° (200), 70.8°(203) confirms hexagonal phase structure of $MoSe_2$ film (JCPDS card no. 29-0914) [48], [100]. Raman Spectroscopy was also performed at room temperature for analyzing its in-plane and out-of-plane components using a 532 nm laser source. **Figure 2.4** (b) shows Raman Spectroscopy with two distinct peaks at 238 cm^{-1} and 286 cm^{-1}. One is out-of-plane mode i.e. A_{1g} mode at 238 cm^{-1} and another at 286 cm^{-1} is the in-plane mode i.e. E^1_{2g} mode which are in good agreement with the previously reported work[48], [56].

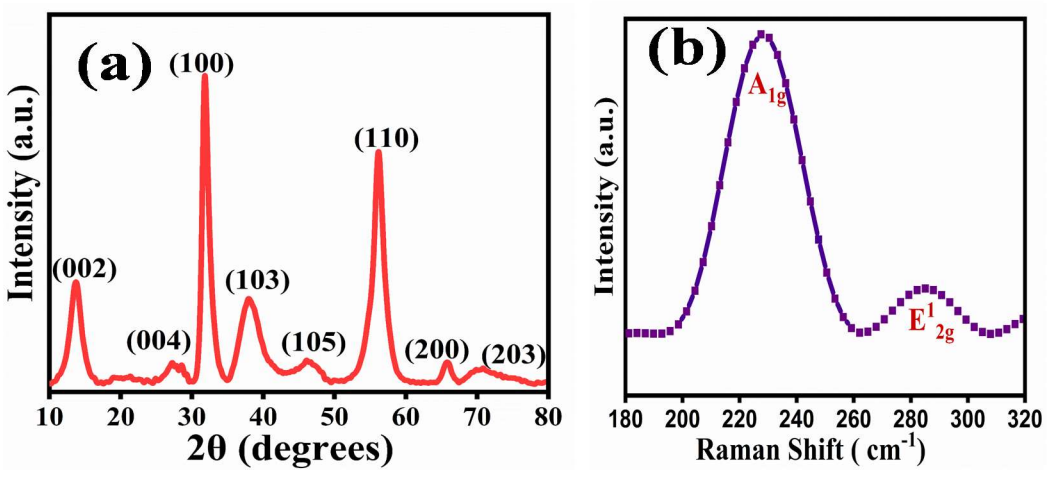

Figure 2.4 (a) XRD pattern; (b) Raman spectrum of the $MoSe_2$.

2.4.2. Optical Characterization of the Device

The thermally grown $MoSe_2$ thin film was characterized for determining its optical absorbance spectrum using V-770 from JASCO, Japan. **Figure 2.5** shows the optical absorbance of the $MoSe_2$ film which depicts the broad absorbance spectral range from 300 nm – 900 nm covering the UV, visible and NIR regions. The inset in **Figure 2.5** shows the Tauc plot for the $MoSe_2$ thin film determining its optical bandgap as 1.96 eV.

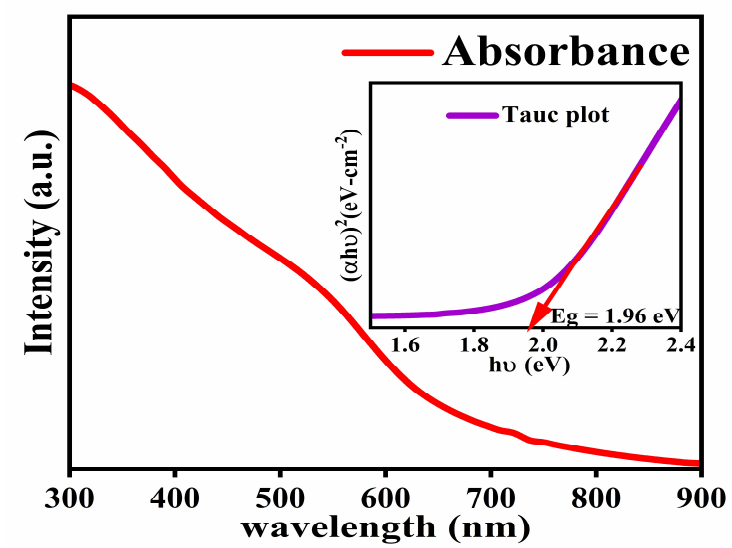

Figure 2.5 Optical absorbance of the film (Inset: Tauc plot).

2.4.3. Optoelectronic Characterization of Fabricated Device

For computing the current-voltage (I-V) characteristics of the fabricated device at room temperature, a semiconductor parameter analyzer (Model: B1500A) system from Keysight, USA was used. Under applied bias voltage from -1.5 V to 1.5 V, the I-V measurement of the fabricated device was performed under dark and white light radiance as shown in **Figure 2.6** (a) and (b) in linear scale and logarithmic scale respectively. A monochromator system as

light source (Model SP2150i, Princeton Instruments) was used for illuminating the active area of the fabricated device for device measurements. From I-V characteristics shown in **Figure 2.6** the symmetric non-linear increase in the current with respect to applied bias voltage is evident hence, confirms formation of schottky junction MSM structure in the fabricated device.

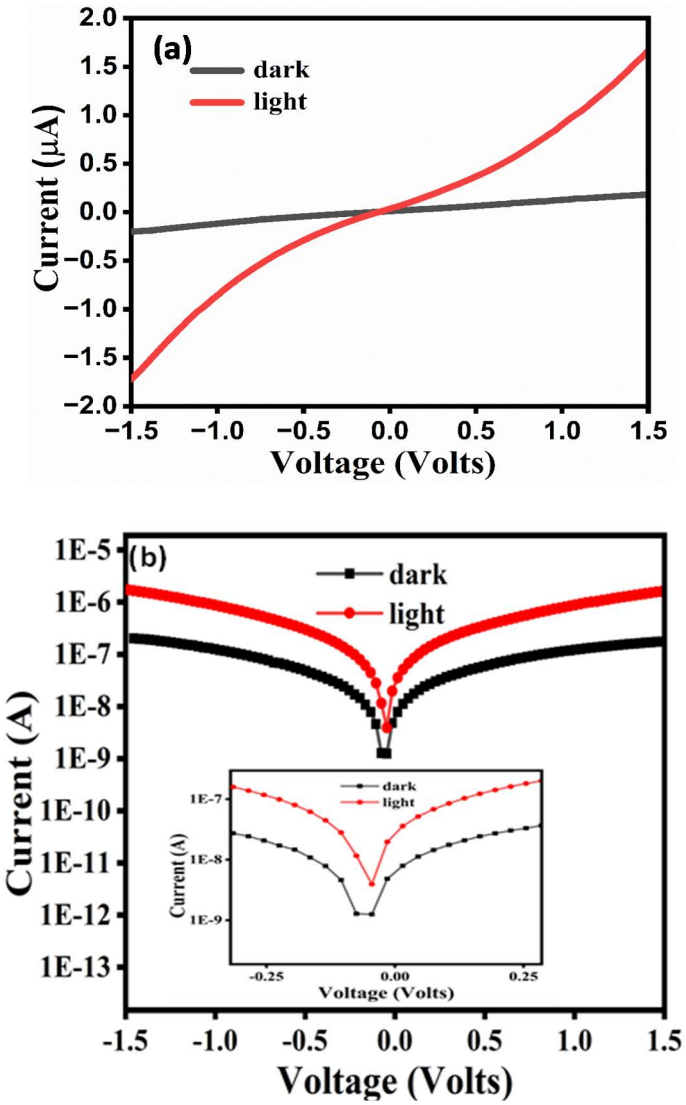

Figure 2.6 I-V characteristics of the fabricated device (a) Linear scale; (b) Logarithmic scale (inset shows the characteristics with magnified scale in the zero bias region).

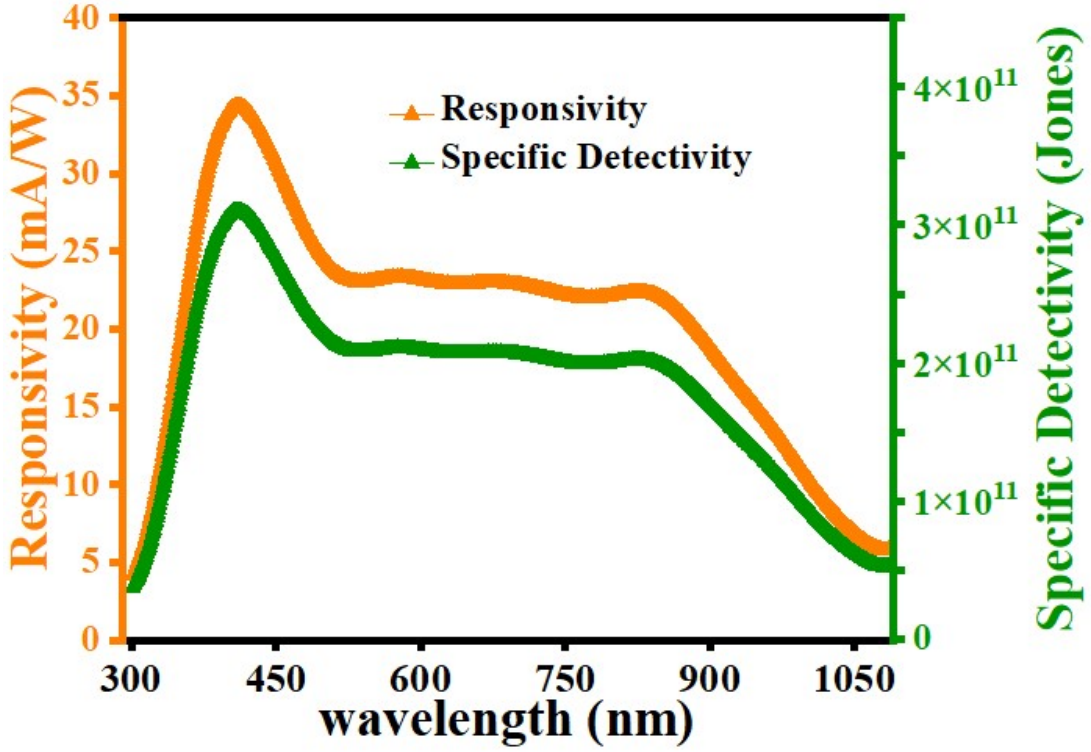

Figure 2.7 Responsivity and Specific detectivity characteristics of the fabricated device.

The fabricated device was further examined for its photoresponse characteristics at room temperature in order to evaluate the key performance parameters of the photodetector including responsivity (R), specific detectivity (D^*) and EQE (%). **Figure 2.7** illustrates the responsivity and specific detectivity of the proposed device measured over the range of 300 nm - 1100 nm.

Responsivity (R) is given by the ratio of the photocurrent produced to the optical power at a given incident light wavelength expressed in A/W. It has following relation[100], [101]:

$$R = \frac{Iph}{Popt} \text{ A/W} \quad (2.1)$$

where, $I_{ph} = I_{ligh} - I_{dark}$ and P_{opt}= incident optical power.

Specific detectivity (D^*) expressed in Jones is measured using following relation[9], [98]:

$$D^* = R \times \sqrt{\frac{A_{eff}}{2 \times e \times I_{dark}}} \text{ Jones} \quad (2.2)$$

where, A_{eff} is the effective area; e is the charge of an electron; I_{dark} is the dark current

External quantum efficiency (EQE) as shown in **Figure 2.8** (a) is formulated as following[4], [6]:

$$\text{EQE (\%)} = 1240*(R/\lambda)*100 \quad (2.3)$$

where R is the responsivity and λ is the incident light wavelength on the device.

Our proposed device showed maximum responsivity of ~50 mA/W, specific detectivity as ~4.5×10^{11} Jones and EQE of ~16% at 415 nm for the applied bias voltage of 1.5 V.

Another important performance parameter of a photodetector is its speed of operation which is determined by transient response characteristics of the fabricated device as shown in **Figure 2.8** (b). Under the applied bias voltage of 1.5 V, change in current was computed with respect to incident pulsed (T_{ON} / T_{OFF}) light on the fabricated device. A pulsed white light with power density of 30 mW/cm^2 was used for device illumination. The rise (fall) time

is the time required by current to rise (fall) from 10% - 90% (90% - 10%) of its maximum value[9], [100]. The rise and fall time is evaluated from the transient response characteristics of the device as 17.76 msec. and 18.38 msec. respectively at room temperature.

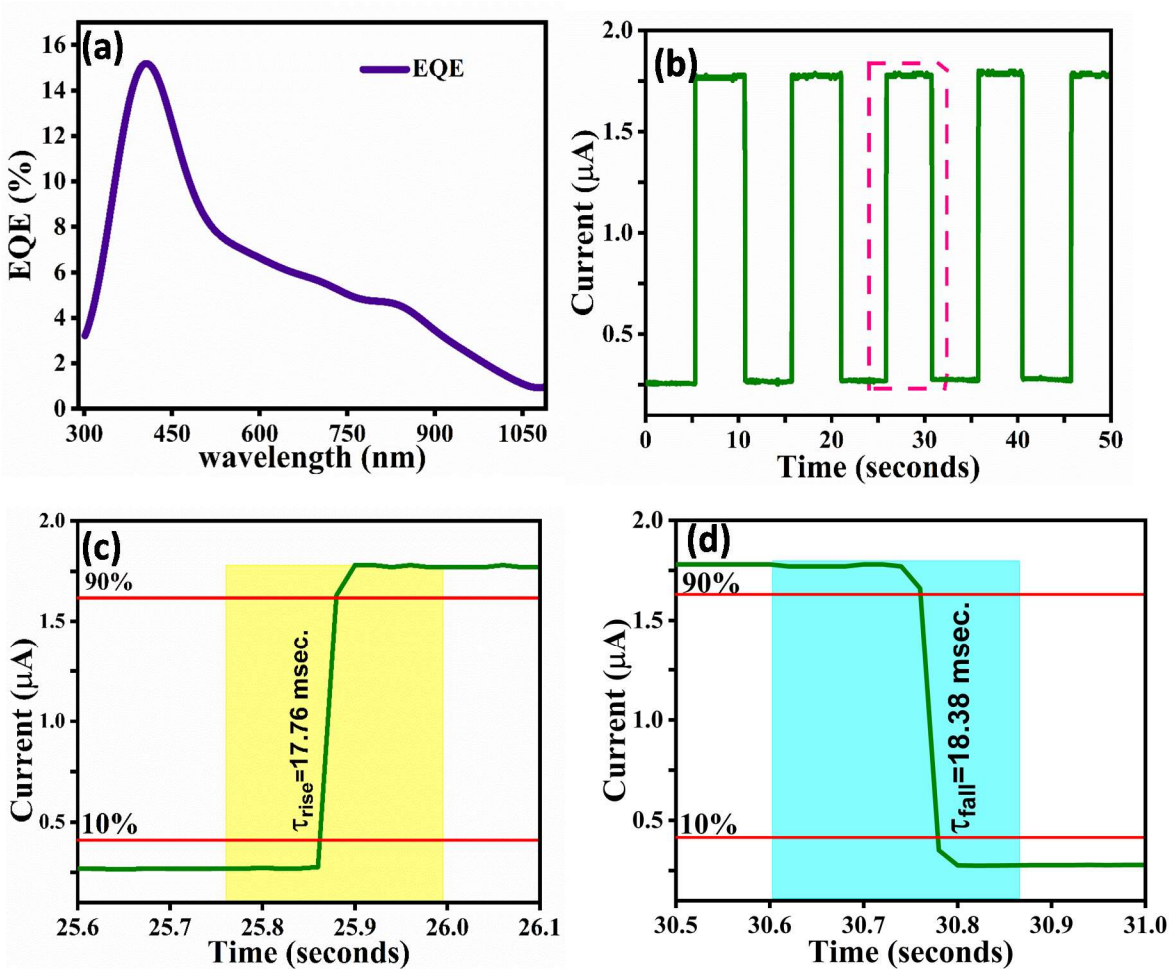

Figure 2.8 (a) EQE plot of the fabricated device; (b) Transient response characteristics of the fabricated device; (c) Rise time calculation of the fabricated device (magnified scale); (d) Fall time calculation of the fabricated device (magnified scale).

We have also investigated the stability of the fabricated device over of period of ~ 8 weeks which is illustrated in **Figure 2.9**. It was observed that there was small deterioration in the device performance i.e. responsivity and specific detectivity over period of time due to uncontrolled open environment characterization of the unpackaged device under study. It may be mentioned that the device performance can be enhanced if fabrication and characterization of the device is done in controlled environment along with its proper packaging.

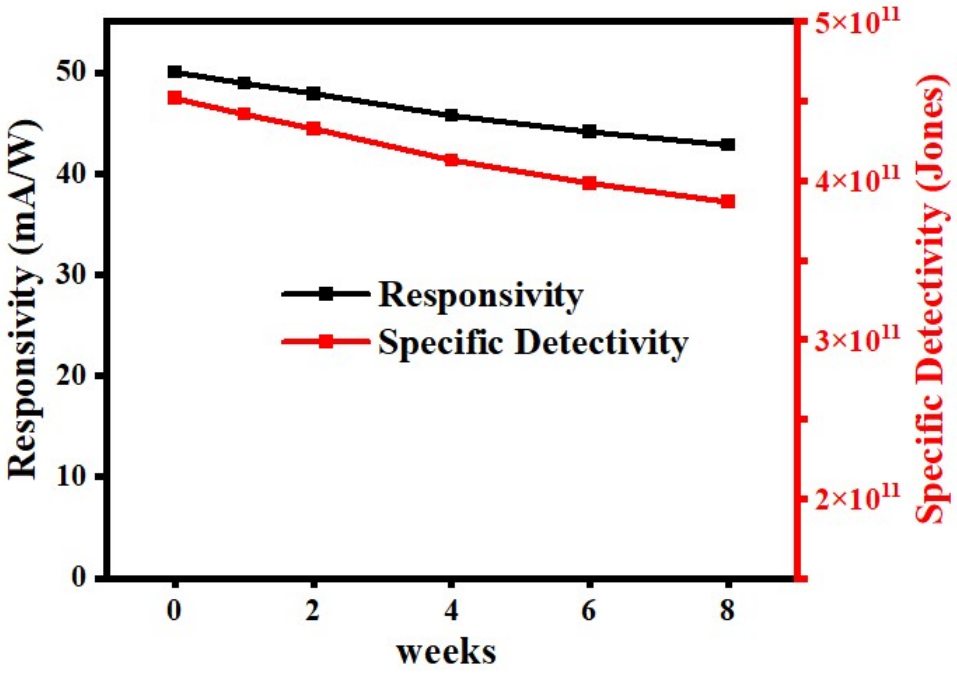

Figure 2.9 Stability analysis in terms of Responsivity and Specific detectivity of the fabricated device over a period of 8 weeks.

2.5 Conclusion

Our proposed work report the Ag/ $MoSe_2$ thin film /Ag based MSM broadband photodetector. A facile cost-effective hydrothermal route was adopted for material synthesis followed by low-cost thermal evaporation technique for thin-film and inter-digitated metal (Ag) electrode deposition. The proposed device structure showed maximum responsivity, specific detectivity and EQE values as ~50 mA/W, ~4.5×10^{11} Jones and ~ 16% respectively at 415 nm under the applied bias voltage of 1.5 V. The rise and fall time computed from transient response were 17.76 msec. and 18.38 msec. respectively at room temperature. Hence, our proposed device shows appreciable photo-response with fast speed of operation which is suitable for optical communication systems.